

Scattering of flexural wave in a thin plate with multiple circular inclusions by using the multipole Trefftz method

Wei-Ming Lee^{1,*}, Jeng-Tzong Chen² and Hung-Ho Hsu¹

¹Department of Mechanical Engineering,

China University of Science and Technology, Taipei, Taiwan

²Department of Harbor and River Engineering,

National Taiwan Ocean University, Keelung, Taiwan

*wmlee@cc.chit.edu.tw

ABSTRACT

The multipole Trefftz method is proposed to solve the scattering of flexural wave by multiple circular inclusions in an infinite thin plate. The near-field dynamic moment concentration factor (DMCF) and the far-field scattering amplitude are determined theoretically. Owing to the addition theorem, the solution represented by multiple coordinates centered at each circle can be transformed into one coordinate centered at one circle where continuity conditions are required. In this way, a coupled infinite linear algebraic system is derived as an analytical model for an infinite thin plate with multiple inclusions subject to incident flexural wave. The formulation is general and is applicable to dealing with the problem containing multiple circular inclusions. Some numerical results are presented in the truncated finite system. The effects of the incident wave number, the thickness of inclusion and the central distance between inclusions on the DMCF and the far-field scattering amplitude are examined. Numerical results show that the DMCF of two inclusions is larger than that of one, when two inclusions are close to each other. The effect of the space between inclusions on the near-field DMCF is different from that on the far-field scattering amplitude.

Keywords: scattering, plate, inclusion, flexural wave, dynamic moment concentration factor, far-field scattering amplitude

1. INTRODUCTION

Thin plates with multiple circular inclusions are commonly observed in engineering structures. These inclusions, or inhomogeneous materials, usually take place in terms of discontinuity such as thickness reduction due to corrosion, or strength degradation resulted by delamination. The deformation and corresponding stresses induced by dynamic loading are propagated throughout the structure by means of wave. At the near field of inclusion (or scatterer), flexural wave scattered in all directions recursively interacts with the incident wave. It turns out that the scattering of the stress wave induces dynamic stress concentration [1] which results in fatigue failure and reduces the loading capacity.

On the other hand, certain applications of the far-field scattering flexural response can be found in vibration analysis or structural health-monitoring system such as the non-destructive inspection.

Nishimura and Jimbo [2] are two pioneers for the analytical study of the dynamic stress concentration. Pao [3] studied the scattering of flexural waves and dynamic stress concentrations around a circular hole, and proposed an analytical solution. Since then, most research work has focused on the scattering of elastic wave and the resulted dynamic stress concentration and has led to a rapid development of analytical or numerical approach [1].

Norris and Vemula [4] considered the scattering of flexural waves by circular inclusions with different plate properties. Squire and Dixon [5] applied the wave function expansion method to study the scattering properties of a single coated cylindrical anomaly located in a thin plate on which flexural waves propagate. Wang [6] presented a theoretical and experimental investigation of the scattering behavior of extensional and flexural plate waves by a cylindrical inhomogeneity. Peng [7] investigated flexural wave scattering and dynamic stress concentration in a heterogeneous plate with multiple cylindrical patches by using acoustical wave propagator technique. The predicted result of the principal stress was compared with the exact solution in a thin plate without patches. Nevertheless, predicted results of dynamic stress concentration were not verified by any independent method. From literature reviews stated previously, few papers except [7] have been published to date reporting the scattering of flexural wave in plate with more than one inclusion.

The Trefftz method was first presented by Trefftz [8]. By using boundary nodes, this method was proposed to construct the solution space using trial complete functions which satisfy the given governing equation [9]. Apparently, Trefftz method is categorized as the boundary-type solution such as the boundary element method (BEM) or boundary integral equation method (BIEM) which can reduce the dimension of the original problem by one and thus the number of the unknowns is much less than that of the domain type methods such as FDM or FEM. Moreover, the Trefftz formulation is

regular and free of calculating improper boundary integrals. However, almost all the problems solved by using Trefftz method are limited in the simply-connected domain. An extension to problems with multiple inclusions, i.e. multiply-connected domain, is our concern in this paper.

The concept of multipole method to solve multiply scattering problems was firstly devised by [10] and used for the interaction of waves with arrays of circular cylinders by Linton and Evans [11]. Recently, one monograph by Martin [12] used these and other methods to solve problems of the multiple scattering in acoustics, electromagnetism, seismology and hydrodynamics. However, the biHelmholtz problem with the fourth order differential equation was not mentioned therein.

This paper proposed the multipole Trefftz method to solve flexural waves scattered by multiple circular inclusions in an analytical way. A coupled infinite system of simultaneous linear algebraic equations is derived as an analytical model for the problem considered here. Some numerical results are presented in the truncated finite system. Once the displacement fields of both infinite plate and inclusions are solved, the near-field DMCF and the far-field scattering amplitude can be determined theoretically. The effects of the central distance, the incident wave number and the thickness of flexible inclusion on the near-field DMCF and the far-field scattering amplitude are examined in this paper.

2. PROBLEM STATEMENT OF SCATTERING OF FLEXURAL WAVE

An infinite thin plate with H nonoverlapping circular inclusions subjected to the incident flexural wave is shown in Figure 1, where $H+1$ observer coordinate systems are used: (x_1, x_2) are the global plane Cartesian coordinates centered at O , (ρ_p, ϕ_p) , $p=1, \dots, H$, are local plane polar coordinates centered at O_p . The radius of the p th circular hole is denoted by R_p and B_p is its corresponding boundary.

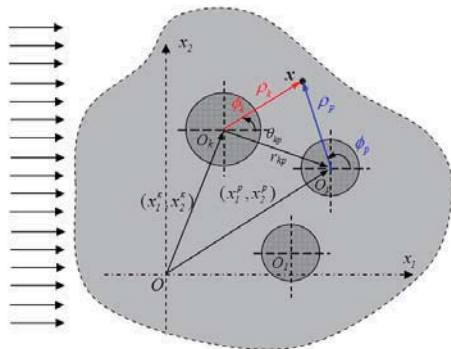


Figure 1 Problem statement for an infinite thin plate with multiple circular inclusions subject to an incident flexural wave

For time-harmonic motion, the governing equation of motion for the plate is

$$\nabla^4 w(\mathbf{x}) - k^4 w(\mathbf{x}) = 0, \quad \mathbf{x} \in \Omega^e, \quad (1)$$

where \mathbf{x} is the field point, Ω^e is the unbounded exterior

region occupied by the infinite plate, ∇^4 is the biharmonic operator, $k^4 = \omega^2 \rho_0 h_0 / D$, k is the wave number, ρ_0 is the volume density, h_0 is the plate thickness, $D = Eh_0^3/12(1-\mu^2)$ is the flexural rigidity of the plate, E denotes the Young's modulus and μ is the Poisson's ratio.

The solution of Eq. (1) in the plane polar coordinates can be represented as

$$w(\rho, \phi) = \sum_{m=-\infty}^{\infty} \tilde{w}_m(\rho) e^{im\phi}, \quad (2)$$

where $\tilde{w}_m(\rho)$ is defined by

$$\tilde{w}_m(\rho) = \tilde{c}_1 J_m(k\rho) + \tilde{c}_2 Y_m(k\rho) + \tilde{c}_3 I_m(k\rho) + \tilde{c}_4 K_m(k\rho), \quad (3)$$

in which \tilde{c}_i ($i=1-4$) are the coefficients, J_m and Y_m are the m th order Bessel functions; and I_m and K_m are the m th order modified Bessel functions. Based on the characteristics of functions at $\rho=0$ and $\rho \rightarrow \infty$, the appropriate Bessel function and the modified Bessel function are chosen to represent the transverse displacement field for the infinite plate and finite inclusion.

An incident flexural wave with an incident angle α with respect to the x_1 axis is represented by

$$w^{(i)}(\rho_p, \phi_p) = w_0 c_p e^{ik\rho_p \cos(\phi_p - \alpha)}, \quad p = 1, \dots, H \quad (4)$$

where $c_p = e^{ik(x_1^p \cos \alpha + x_2^p \sin \alpha)}$ is a phase factor associated with the p th circular inclusion [11] of which the coordinates of the center are (x_1^p, x_2^p) . From the Jacobi's expansion [13], Eq. (4) can be expanded in a series form

$$w^{(i)}(\rho_p, \phi_p) = \sum_{m=-\infty}^{\infty} a_m^{(i)}(k\rho_p) e^{im\phi_p}, \quad p = 1, \dots, H \quad (5)$$

where $a_m^{(i)}(k\rho_p) = w_0 c_p i^m J_m(k\rho_p) e^{-im\alpha}$.

Based on the displacement field, the normal bending slope, normal bending moment, tangential bending moment and effective shear force can be derived by applying the following operators with respect to the field point,

$$K_\theta(\cdot) = \frac{\partial(\cdot)}{\partial \rho}, \quad (6)$$

$$K_{m_n}(\cdot) = -D \left[\mu \nabla^2(\cdot) + (1-\mu) \frac{\partial^2(\cdot)}{\partial \rho^2} \right], \quad (7)$$

$$K_{m_t}(\cdot) = -D \left[\nabla^2(\cdot) + (\mu-1) \frac{\partial^2(\cdot)}{\partial \rho^2} \right], \quad (8)$$

$$K_s(\cdot) = -D \left[\frac{\partial}{\partial \rho} (\nabla^2(\cdot)) + (1-\mu) \left(\frac{1}{\rho} \right) \frac{\partial}{\partial \phi} \left[\frac{\partial}{\partial \rho} \left(\frac{1}{\rho} \frac{\partial(\cdot)}{\partial \phi} \right) \right] \right], \quad (9)$$

3. ANALYTICAL DERIVATIONS FOR FLEXURAL WAVE SCATTERED BY MULTIPLE CIRCULAR INCLUSIONS

Assume that a time harmonic incident flexural wave impinges on an infinite thin plate containing H circular inclusions as shown in Figure 1. The problem of flexural wave scattered by H circular inclusions is to solve Eq. (1) subject to the continuity conditions along each interface

between the plate and inclusions and a radiation condition at infinity, i.e. the scattered field equaling to zero when $\rho \rightarrow \infty$. Based on Eq. (2), the scattered field of plate can be expressed as an infinite sum of multipole at the center of each circular inclusion as follows:

$$w^{sc}(\mathbf{x}; \rho_1, \phi_1, \dots, \rho_H, \phi_H) = \sum_{k=1}^H \left[\sum_{m=-\infty}^{\infty} a_m^k H_m^{(1)}(k\rho_k) e^{im\phi_k} + b_m^k K_m(k\rho_k) e^{im\phi_k} \right] \quad (10)$$

where $(\rho_1, \phi_1), \dots, (\rho_H, \phi_H)$ are the polar coordinates of the field point \mathbf{x} with respect to each center of circular inclusion. The Hankel function ($J+iY$) and the modified Bessel function K are chosen to represent an infinite plate due to their values being finite as $\rho \rightarrow \infty$. Considering the incident wave, the displacement field of the plate is defined by

$$w(\mathbf{x}) = w^{(i)}(\mathbf{x}) + w^{sc}(\mathbf{x}) \quad (11)$$

Similarly, from Eq. (2), the displacement field of the p th inclusion is expressed as, $p=1, \dots, H$,

$$w_p^i(\mathbf{x}; \rho_p, \phi_p) = \sum_{m=-\infty}^{\infty} \left(c_m^p J_m(k\rho_p) e^{im\phi_p} + d_m^p I_m(k\rho_p) e^{im\phi_p} \right) \quad (12)$$

The Bessel function J and the modified Bessel function I are chosen to represent a finite inclusion due to their values being finite at $\rho=0$. The coefficients of a_m^k, b_m^k, c_m^k and $d_m^k, k=1, \dots, H; m=0, \pm 1, \pm 2, \dots$, can be determined by the following continuity conditions, $\rho_p = R_p, 0 \leq \phi_p \leq 2\pi, p=1, \dots, H$,

$$w(\rho_p, \phi_p) = w_p^i(\rho_p, \phi_p), \quad (13)$$

$$\theta(\rho_p, \phi_p) = \theta_p^i(\rho_p, \phi_p), \quad (14)$$

$$m(\rho_p, \phi_p) = m_p^i(\rho_p, \phi_p), \quad (15)$$

$$v(\rho_p, \phi_p) = v_p^i(\rho_p, \phi_p). \quad (16)$$

For the p th circular interface, substituting both Eq. (11) and Eq. (12) into Eq. (13) yields

$$\sum_{m=-\infty}^{\infty} a_m^{(i)}(k\rho_p) e^{im\phi_p} + \sum_{k=1}^H \left[\sum_{m=-\infty}^{\infty} a_m^k H_m^{(1)}(k\rho_k) e^{im\phi_k} + b_m^k K_m(k\rho_k) e^{im\phi_k} \right] - \sum_{m=-\infty}^{\infty} \left(c_m^p J_m(k\rho_p) e^{im\phi_p} + d_m^p I_m(k\rho_p) e^{im\phi_p} \right) = 0 \quad (17)$$

To determine these unknown coefficients, the other three equations (14)-(16) are required by applying three operators of Eqs.(6), (7) and (9) to Eq.(17). For one thing, this procedure involves the higher order derivatives. For another thing, Equation (17) consists of several different variables. Therefore, it is difficult to put into practice. This question can be answered by using the addition theorem [13] which will be described in the following.

Based on the Graf's addition theorem for the Bessel functions, we can express the theorem in the following form,

$$J_m(k\rho_k) e^{im\phi_k} = \sum_{n=-\infty}^{\infty} J_{m-n}(kr_{kp}) e^{i(m-n)\theta_{kp}} J_n(k\rho_p) e^{in\phi_p} \quad (18)$$

$$I_m(k\rho_k) e^{im\phi_k} = \sum_{n=-\infty}^{\infty} I_{m-n}(kr_{kp}) e^{i(m-n)\theta_{kp}} I_n(k\rho_p) e^{in\phi_p} \quad (19)$$

$$H_m^{(1)}(k\rho_k) e^{im\phi_k} = \begin{cases} \sum_{n=-\infty}^{\infty} H_{m-n}^{(1)}(kr_{kp}) e^{i(m-n)\theta_{kp}} J_n(k\rho_p) e^{in\phi_p}, & \rho_p < r_{kp} \\ \sum_{n=-\infty}^{\infty} J_{m-n}(kr_{kp}) e^{i(m-n)\theta_{kp}} H_n^{(1)}(k\rho_p) e^{in\phi_p}, & \rho_p > r_{kp} \end{cases} \quad (20)$$

$$K_m(k\rho_k) e^{im\phi_k} = \begin{cases} \sum_{n=-\infty}^{\infty} (-1)^n K_{m-n}(kr_{kp}) e^{i(m-n)\theta_{kp}} I_n(k\rho_p) e^{in\phi_p}, & \rho_p < r_{kp} \\ \sum_{n=-\infty}^{\infty} (-1)^{m-n} I_{m-n}(kr_{kp}) e^{i(m-n)\theta_{kp}} K_n(k\rho_p) e^{in\phi_p}, & \rho_p > r_{kp} \end{cases} \quad (21)$$

where (ρ_p, ϕ_p) and (ρ_k, ϕ_k) as shown in Figure 1 are the polar coordinates of the field point \mathbf{x} with respect to O_p and O_k , respectively, which are the origins of two polar coordinate systems and (r_{kp}, θ_{kp}) are the polar coordinates of O_p with respect to O_k .

By substituting the addition theorem for the Bessel functions $H_m^{(1)}(k\rho_k)$ and $K_m(k\rho_k)$ into Eq. (17), only the p th coordinate system is involved and then the displacement continuity condition in the circular boundary B_p ($p=1, \dots, H$) for the case of $\rho_p < r_{kp}$ is given by

$$\sum_{m=-\infty}^{\infty} a_m^{(i)}(k\rho_p) e^{im\phi_p} + \left[\sum_{m=-\infty}^{\infty} a_m^p H_m^{(1)}(k\rho_p) + \sum_{m=-\infty}^{\infty} b_m^p K_m(k\rho_p) \right] e^{im\phi_p} + \sum_{\substack{k=1 \\ k \neq p}}^H \left[\sum_{m=-\infty}^{\infty} a_m^k \sum_{n=-\infty}^{\infty} H_{m-n}^{(1)}(kr_{kp}) e^{i(m-n)\theta_{kp}} J_n(k\rho_p) + \sum_{m=-\infty}^{\infty} b_m^k \sum_{n=-\infty}^{\infty} (-1)^n K_{m-n}(kr_{kp}) e^{i(m-n)\theta_{kp}} I_n(k\rho_p) \right] e^{im\phi_p} - \sum_{m=-\infty}^{\infty} \left(c_m^p J_m(k\rho_p) e^{im\phi_p} + d_m^p I_m(k\rho_p) e^{im\phi_p} \right) = 0 \quad (22)$$

Furthermore, it can be rewritten as

$$\sum_{m=-\infty}^{\infty} e^{im\phi_p} \left\{ H_m^{(1)}(k\rho_p) a_m^p + K_m(k\rho_p) b_m^p + \sum_{\substack{k=1 \\ k \neq p}}^H \left[\sum_{n=-\infty}^{\infty} A_{mn}^k(k\rho_p) a_n^k + \sum_{n=-\infty}^{\infty} B_{mn}^k(k\rho_p) b_n^k \right] - J_m(k\rho_p) c_m^p - I_m(k\rho_p) d_m^p + a_m^{(i)}(k\rho_p) \right\} = 0 \quad (23)$$

where

$$A_{mn}^k(k\rho_p) = H_{n-m}^{(1)}(kr_{kp}) e^{i(n-m)\theta_{kp}} J_m(k\rho_p) \quad (24)$$

$$B_{mn}^k(k\rho_p) = (-1)^m e^{i(n-m)\theta_{kp}} I_m(k\rho_p) K_{n-m}(kr_{kp}) \quad (25)$$

By applying Eq. (6) to Eq. (23), the normal slope continuity condition in the circular boundary B_p ($p=1, \dots, H$) is given by

$$\sum_{m=-\infty}^{\infty} e^{im\phi_p} k \left\{ H_m^{(1)'}(k\rho_p) a_m^p + K_m'(k\rho_p) b_m^p + \sum_{\substack{k=1 \\ k \neq p}}^H \left[\sum_{n=-\infty}^{\infty} C_{mn}^k(k\rho_p) a_n^k + \sum_{n=-\infty}^{\infty} D_{mn}^k(k\rho_p) b_n^k \right] - J_m'(k\rho_p) c_m^p - I_m'(k\rho_p) d_m^p + b_m^{(i)}(k\rho_p) \right\} = 0 \quad (26)$$

where

$$C_{mn}^k(k\rho_p) = H_{n-m}^{(1)}(kr_{kp}) e^{i(n-m)\theta_{kp}} J_m'(k\rho_p) \quad (27)$$

$$D_{mn}^k(k\rho_p) = (-1)^m e^{i(n-m)\theta_{kp}} I_m'(k\rho_p) K_{n-m}(kr_{kp}) \quad (28)$$

$$b_m^{(i)}(k\rho_p) = c_p^i J_m'(k\rho_p) e^{-im\alpha} \quad (29)$$

By using Eq. (15), the normal bending moment continuity condition in the circular boundary B_p ($p=1, \dots, H$) yields

$$\sum_{m=-\infty}^{\infty} e^{im\phi_p} \{ \alpha_m^H(k\rho_p) a_m^p + \alpha_m^K(k\rho_p) b_m^p + \sum_{\substack{k=1 \\ k \neq p}}^H \left[\sum_{n=-\infty}^{\infty} E_{mn}^k(k\rho_p) a_n^k + \sum_{n=-\infty}^{\infty} F_{mn}^k(k\rho_p) b_n^k \right] - \alpha_m^J(k\rho_p) c_m^p - \alpha_m^I(k\rho_p) d_m^p + c_m^{(i)}(k\rho_p) \} = 0 \quad (30)$$

where

$$E_{mn}^k(k\rho_p) = H_{n-m}^{(1)}(kr_{kp}) e^{i(n-m)\theta_{kp}} \alpha_m^J(k\rho_p) \quad (31)$$

$$F_{mn}^k(k\rho_p) = (-1)^m e^{i(n-m)\theta_{kp}} \alpha_m^I(k\rho_p) K_{n-m}(kr_{kp}) \quad (32)$$

$$c_m^{(i)}(k\rho_p) = c_p^i \alpha_m^J(k\rho_p) e^{-im\alpha} \quad (33)$$

in which the moment operator $\alpha_m^X(k\rho)$ from Eq. (7) is defined as

$$\alpha_m^X(k\rho) = D \left\{ (1-\mu) \frac{X'_m(k\rho)}{\rho} - \left[(1-\mu) \frac{m^2}{\rho^2} \mp k^2 \right] X_m(k\rho) \right\} \quad (34)$$

where the upper (lower) signs refer to $X = J, Y, H, (I, K)$, respectively. The differential equations for the Bessel functions have been used to simplify $\alpha_m^X(k\rho)$.

Similarly, the effective shear operator $\beta_m^X(k\rho)$ derived from Eq. (9) can be expressed as,

$$\beta_m^X(k\rho) = D \left\{ [m^2(1-\mu) \pm (k\rho)^2] \frac{X'_m(k\rho)}{\rho^2} - m^2(1-\mu) \frac{X_m(k\rho)}{\rho^3} \right\}, \quad (35)$$

and the effective shear force continuity condition in the circular boundary B_p ($p=1, \dots, H$) is given by

$$\sum_{m=-\infty}^{\infty} e^{im\phi_p} \{ \beta_m^H(k\rho_p) a_m^p + \beta_m^K(k\rho_p) b_m^p + \sum_{\substack{k=1 \\ k \neq p}}^H \left[\sum_{n=-\infty}^{\infty} E_{mn}^k(k\rho_p) a_n^k + \sum_{n=-\infty}^{\infty} F_{mn}^k(k\rho_p) b_n^k \right] - \beta_m^J(k\rho_p) c_m^p - \beta_m^I(k\rho_p) d_m^p + d_m^{(i)}(k\rho_p) \} = 0 \quad (36)$$

where $G_{mn}^k(k\rho_p)$, $H_{mn}^k(k\rho_p)$ and $d_m^{(i)}(k\rho_p)$ are determined by replacing $\alpha_m^X(k\rho_p)$ in Eqs. (31)-(33) with $\beta_m^X(k\rho_p)$, respectively.

Applying the orthogonal property of $\{ e^{im\phi_p} \}$ to Eqs. (23), (26), (30) and (36), respectively, and setting ρ_p to R_p give

$$\begin{cases} H_m^{(1)}(kR_p) a_m^p + K_m(kR_p) b_m^p + \sum_{\substack{k=1 \\ k \neq p}}^H \left[\sum_{n=-\infty}^{\infty} A_{mn}^k(kR_p) a_n^k + \sum_{n=-\infty}^{\infty} B_{mn}^k(kR_p) b_n^k \right] - J_m(kR_p) c_m^p - I_m(kR_p) d_m^p = -a_m^{(i)}(kR_p), \\ H_m^{(1)'}(kR_p) a_m^p + K'_m(kR_p) b_m^p + \sum_{\substack{k=1 \\ k \neq p}}^H \left[\sum_{n=-\infty}^{\infty} C_{mn}^k(kR_p) a_n^k + \sum_{n=-\infty}^{\infty} D_{mn}^k(kR_p) b_n^k \right] - J'_m(kR_p) c_m^p - I'_m(kR_p) d_m^p = -b_m^{(i)}(kR_p), \\ \alpha_m^H(kR_p) a_m^p + \alpha_m^K(kR_p) b_m^p + \sum_{\substack{k=1 \\ k \neq p}}^H \left[\sum_{n=-\infty}^{\infty} E_{mn}^k(kR_p) a_n^k + \sum_{n=-\infty}^{\infty} F_{mn}^k(kR_p) b_n^k \right] - \alpha_m^J(kR_p) c_m^p - \alpha_m^I(kR_p) d_m^p = -c_m^{(i)}(kR_p), \\ \beta_m^H(kR_p) a_m^p + \beta_m^K(kR_p) b_m^p + \sum_{\substack{k=1 \\ k \neq p}}^H \left[\sum_{n=-\infty}^{\infty} G_{mn}^k(kR_p) a_n^k + \sum_{n=-\infty}^{\infty} H_{mn}^k(kR_p) b_n^k \right] - \beta_m^J(kR_p) c_m^p - \beta_m^I(kR_p) d_m^p = -d_m^{(i)}(kR_p), \end{cases} \quad (37)$$

for $m=0, \pm 1, \pm 2, \dots, n=0, \pm 1, \pm 2, \dots$, and $p = 1, \dots, H$. Equation (37) is a coupled infinite system of simultaneous linear algebraic equations which is the

analytical model for the flexural scattering of an infinite plate containing multiple circular inclusions. In order to present the numerical results in the following section, the infinite system of Eq. (37) is truncated to a $(4H)(2M+1)$ system of equations for $(4H)(2M+1)$ unknown coefficients, i.e. $m=0, \pm 1, \pm 2, \dots, \pm M$. Once the coefficients a_m^k , b_m^k , c_m^k and d_m^k ($k=1, \dots, H$; $m=0, \pm 1, \pm 2, \dots, \pm M$) are determined, the displacement fields of an infinite plate and inclusions can be both determined by substituting them into Eqs. (11) and (12).

3.1 Dynamic moment concentration factors

In the polar coordinates, bending slope, the normal bending moment, tangential bending moment and effective shear force of an infinite plate and each inclusion induced by the incident wave can be determined by substituting Eqs. (11) and (12) into Eqs. (6)-(9), respectively. By setting the amplitude of incident wave to be one ($w_0=1$), the amplitude of normal bending moment produced by the incident wave is

$$M_0 = Dk^2. \quad (38)$$

The dynamic moment concentration factor (DMCF) at any field point x is defined as

$$\text{DMCF}(x) = m_t(x) / M_0 \quad (39)$$

where the tangential bending moment $m_t(x)$ is determined by the following equations.

$$m_t(\rho_p, \phi_p) = \begin{cases} \sum_{m=-\infty}^{\infty} e^{im\phi_p} \{ f_m^{(i)}(k\rho_p) + \gamma_m^H(k\rho_p) a_m^p + \gamma_m^K(k\rho_p) b_m^p + \sum_{\substack{k=1 \\ k \neq p}}^H \left[\sum_{n=-\infty}^{\infty} \bar{E}_{mn}^k(k\rho_p) a_n^k + \bar{F}_{mn}^k(k\rho_p) b_n^k \right] \}, & \text{for the plate} \\ \sum_{m=-\infty}^{\infty} e^{im\phi_p} \{ \gamma_m^J(k\rho_p) c_m^p + \gamma_m^I(k\rho_p) d_m^p \}, & \text{for the inclusion} \end{cases} \quad (40)$$

where $\bar{E}_{mn}^k(k\rho_p)$, $\bar{F}_{mn}^k(k\rho_p)$ and $f_m^{(i)}(k\rho_p)$ are obtained by replacing $\alpha_m^X(k\rho_p)$ in Eqs. (31)-(33) with $\gamma_m^X(k\rho_p)$, respectively, and the tangential bending moment operator $\gamma_m^X(k\rho)$ derived from Eq. (8) is given by

$$\gamma_m^X(k\rho) = D \left\{ (\mu-1) \frac{X'_m(k\rho)}{\rho} - \left[(\mu-1) \frac{m^2}{\rho^2} \mp k^2 \right] X_m(k\rho) \right\}. \quad (41)$$

3.2 Scattered far-field amplitude

For the most part of scattering applications, it is interesting to measure the scattered field far away from the scatter. On the other hand, the asymptotic behavior or uniqueness of fundamental solutions is an important issue for the numerical computation. Therefore, we examine the behavior of the scattered response in the far field. In this paper, the scattered far-field amplitude $f(\phi)$ [4] is defined as

$$f(\phi) = \lim_{\rho \rightarrow \infty} \sqrt{2\rho} \cdot |w^{sc}(x)|, \quad (42)$$

where the radius of the field point ρ is taken 90m because $f(\phi)$ converges a steady value when this

radius is more than about 90m.

4. NUMERICAL RESULTS AND DISCUSSIONS

To verify the proposed method, the FORTRAN code was implemented to solve the flexural wave scattered by multiple circular inclusions in an infinite thin plate. The DMCF as well as the far-field scattering amplitude is theoretically derived and numerically determined in this paper. In all cases, the thickness of plate h_0 is 0.002m unless otherwise specified. The following dimensionless variables are utilized in the computation: the incident wave number is ka , the space between inclusions is L/a and the thickness of flexible inclusion is h/h_0 , where a is the radius of a circular inclusion and L is the central distance between inclusions. For the special case of a hole, it can be modeled by using h/h_0 to be 0.0005 in the numerical computation. To obtain the more accurate results in the case of one inclusion, the required number of M truncated in the finite system is taken 10. For the case of two inclusions, numerical experiments show that the required number of M mainly depends on the space between inclusions to be considered. Only when does its value become large such as 4.0, the required number of M can be reduced when the incident wave number is small. It shows that the required number of M can be taken from 20 to 10 for the dimensionless central distance L/a ranged from 2.1 to 4.0.

Case 1: An infinite plate with one circular inclusion [4]

An infinite plate with one circular inclusion of radius $R_1=1$ subject to the incident flexural wave with $\alpha=0$ was firstly considered. For the case of $ka=0.005$ and $h/h_0=0.0005$, Fig. 2 shows the distribution of DMCF on the circular boundary. The maximum of DMCF occurs at $\phi=\pi/2, -\pi/2$ and its value is 1.8514 which agrees with the analytical solution of an infinite plate with one hole[1].

Figure 3 shows the distribution of DMCF on the circular boundary when the different incident wave numbers ($ka=0.5, 1.0$ and 3.0) and the different thicknesses of inclusion ($h/h_0=0.0005, 0.5$ and 0.75) are considered. Since the angle of incident wave is zero, $\alpha=0$, its distribution is symmetric to the x-axis. When ka is small, the distribution of DMCF has the symmetry of the y-axis. But this phenomenon is not observed as ka increases. In addition, the distribution of DMCF gradually changes to backward scattering from forward scattering as h/h_0 decreases, especially when ka is large as shown in Fig.3 (a). In general, the magnitude of DMCF increases as the h/h_0 decreases. But it is not the case for some azimuthal coordinates as ka increases i.e. the dynamic behavior is obvious. Figure 4 shows the far field backscattering amplitude versus the dimensionless wave number. As h/h_0 decreases, the ka occurred at first trough decreases, the far-field amplitude increase and its curve becomes gently eventually. The proposed results match well with those reported in [4]. It can be found that the amplitude for the scattering response in the far field is $O(\rho^{-1/2})$ to satisfy the radiation condition.

Case 2: An infinite plate with two circular inclusions

The case of two identical flexible inclusions was considered in Fig. 5. For $L/a=2.1$, Fig. 6 shows the distribution of DMCF on the circular boundary B_1 when the different incident dimensionless wave numbers ($ka=0.5, 1.0$ and 3.0) and the different dimensionless thicknesses of inclusion ($h/h_0=0.0005, 0.5$ and 0.75) are considered. It is observed that the distribution of DMCF of two circular inclusions is different from that of one, where the maximum of DMCF increases nearly three times since the two inclusions are close to each other. In addition to the large magnitude, the symmetry of axis is not observed and the variation along the azimuthal coordinate is significant when ka increases. Figure 7 shows the far field backscattering amplitude versus the dimensionless wave number. Except the case of the hole, the scattering amplitude is similar to that of one. But the amplitude becomes large in this case.

For $L/a=4.0$, Fig. 8 shows the distribution of DMCF on the circular boundary B_1 when the different incident dimensionless wave numbers ($ka=0.5, 1.0$ and 3.0) and the different dimensionless thicknesses of inclusion ($h/h_0=0.0005, 0.5$ and 0.75) are considered. Comparing Fig. 3(a) with Fig. 8(a), the central distance is large enough so that the DMCF distribution of two inclusions is similar to that of one. But the characteristics of far-field are not the case. From Figs. 4, 7, and 9, the far-field amplitude for $L/a=4.0$ is similar to that for $L/a=1.0$ other than that of one.

It is observed that the effect of the space between inclusions on the near-field DMCF is different from that on the far-field scattering amplitude. Only when concerning the DMCF, the multiple scattering can be simplified by the simple scattering when the space between inclusions is large enough. But the prediction of the far-field scattering does not follow this rule.

5. CONCLUSION

The flexural wave scattered by multiple circular inclusions in a thin plate was successively solved by using the multipole Trefftz method with the aid of the addition theorem. The DMCF as well as the scattered far-field amplitude is theoretically derived and numerically determined in this paper. By using the addition theorem, the Trefftz method can be extended to deal with multiply scattering problems. The proposed algorithm is general and easily applicable to problems with multiple inclusions which are not easily solved by using the traditional analytical method. An analytical model for the multiple scattering of the plate problem can be derived as a coupled infinite system of simultaneous equations. Numerical examples in a truncated system are presented. The magnitude of DMCF of two inclusions is larger than that of one when the space of inclusions is small. In general, the magnitude of DMCF increases as h/h_0 decreases. However, it is noted that for some azimuthal coordinates it increases when both h/h_0 and ka increase. The effect of the space between inclusions on the near-field DMCF is different from that on the far-field scattering amplitude. It is helpful to further study the multiple scattering of flexural wave.

6. REFERENCES

- [1] Y.H. Pao and C.C. Mow, *Diffraction of elastic waves and dynamics stress concentration*, Crane-Russak, New York, 1972.
- [2] G. Nishimura and Y. Jimbo, "A dynamical problem of stress concentration," *Journal of the Faculty of Engineering*, University of Tokyo, Japan, vol. 24, pp.101-, 1955.
- [3] Y.H. Pao, "Dynamical stress concentration in an elastic plate," *Transactions of the ASME Journal of Applied Mechanics*, vol. 29, pp. 299-305, 1962.
- [4] A.N. Norris and C. Vemula, "Scattering of flexural waves on thin plates," *Journal of Sound and Vibration*, vol. 181, pp.115-125, 1955.
- [5] V. A. Squire and T. W. Dixon, "Scattering of flexural waves from a coated cylindrical anomaly in a thin plate," *Journal of Sound and Vibration*, vol. 236, no.2, pp. 367-373, 2000.
- [6] C.H. Wang and F.K. Chang, "Scattering of plate waves by a cylindrical inhomogeneity," *Journal of Sound and Vibration*, vol. 282, pp. 429-451, 2005.
- [7] S.Z. Peng, "Flexural wave scattering and dynamic stress concentration in a heterogeneous plate with multiple cylindrical patches by acoustical wave propagator technique," *Journal of Sound and Vibration*, vol. 286, pp. 729-743, 2005.
- [8] E. Trefftz, "Ein Gegenstück zum Ritz' schen Verfahren." *Proc. Second Int. Cong. Appl. Mech.*, Zurich, pp. 131-137, 1926.
- [9] N. Kamiya, and E. Kita, "Trefftz method: an overview," *Advances in Engineering Software*, vol. 24, pp.3-12, 1955.
- [10] F. Závřiska, "Über die Beugung elektromagnetischer Wellen an parallelen, unendlich langen Kreiszyllindern," *Annalen der Physik*, 4 Folge, vol. 40, pp. 1023-1056, 1913.
- [11] C.M. Linton, and D.V. Evans, "The interaction of waves with arrays of vertical circular cylinders," *Journal of Fluid Mechanics*, vol. 215, pp. 549-569, 1999.
- [12] P.A. Martin, *Multiple scattering interaction of time-harmonic wave with N obstacles*, Cambridge University Press, Cambridge, 2006.
- [13] G.N. Watson, *A Treatise on the Theory of Bessel Functions*, second edition. Cambridge: Cambridge Library edition, 1995.

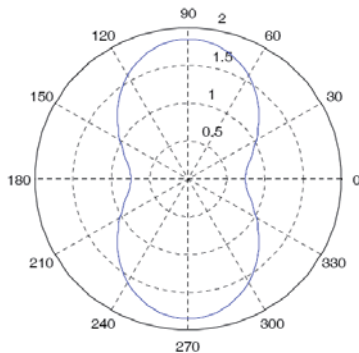


Figure 2 Distribution of DMCF on the circular boundary ($ka=0.005$, $h/h_0=0.0005$)

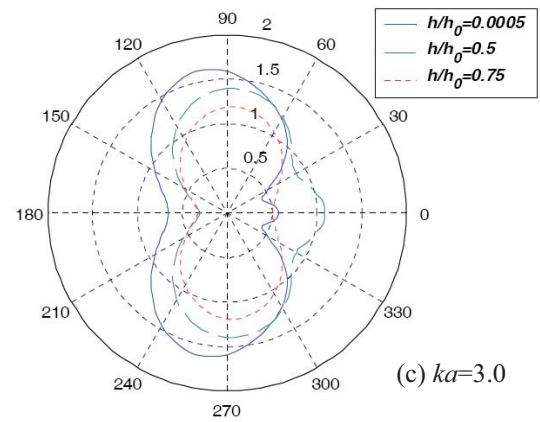
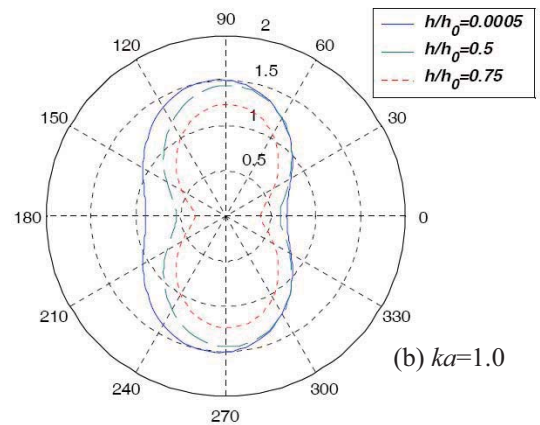
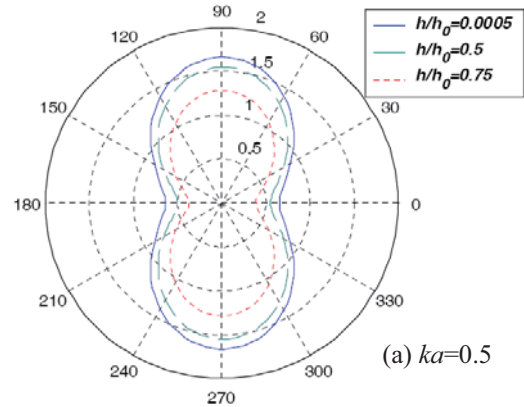


Figure 3 Distribution of DMCF on the circular boundary at different thicknesses of flexible inclusion, solid line for $h/h_0 = 0.0005$, dashed line for $h/h_0 = 0.5$ and dotted line for $h/h_0 = 0.75$, and at different incident wave number (a) $ka=0.5$, (b) $ka=1.0$ and (c) $ka=3.0$

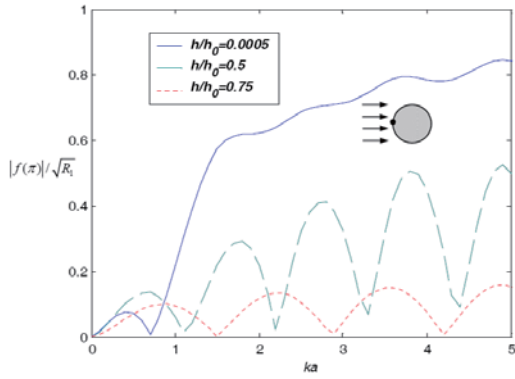


Figure 4 Far-field backscattering amplitude versus the dimensionless wave number at different thicknesses of flexible inclusion, solid line for $h/h_0 = 0.0005$, dashed line for $h/h_0 = 0.5$ and dotted line for $h/h_0 = 0.75$

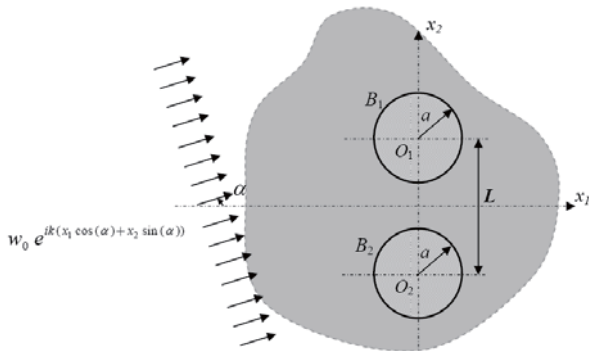


Figure 5 An infinite thin plate with two circular inclusions subject to an incident flexural wave

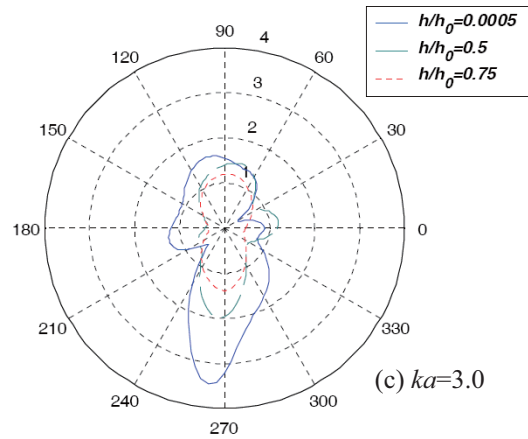
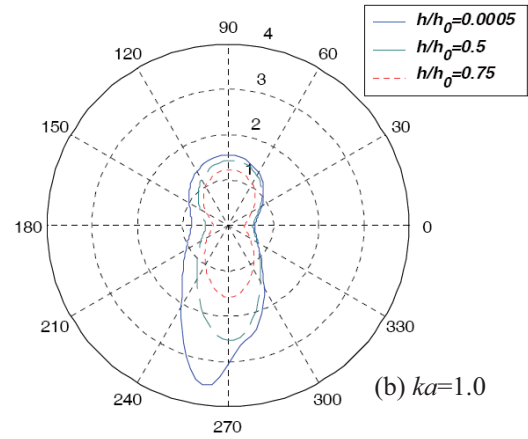
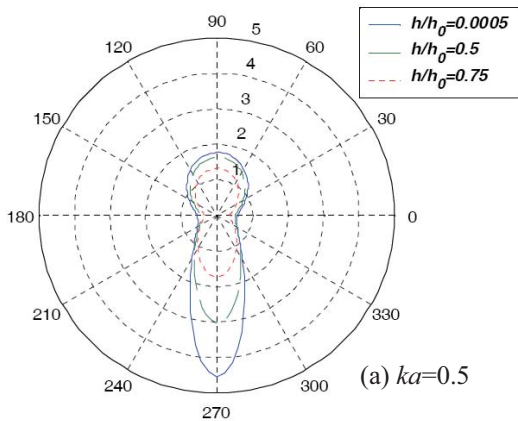


Figure 6 Distribution of DMCF on the first circular boundary B_1 at different thicknesses of flexible inclusion, solid line for $h/h_0 = 0.0005$, dashed line for $h/h_0 = 0.5$ and dotted line for $h/h_0 = 0.75$, and at different incident wave number (a) $ka=0.5$, (b) $ka=1.0$ and (c) $ka=3.0$ ($L/a=2.1$)

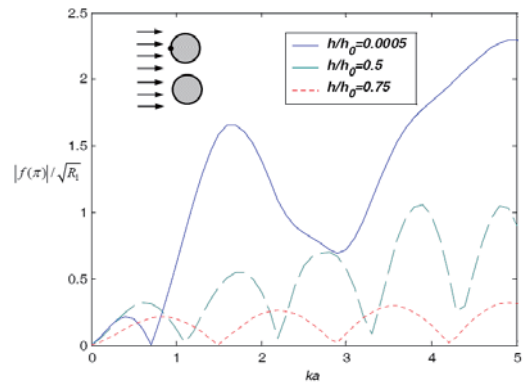


Figure 7 Far-field backscattering amplitude versus the dimensionless wave number at different thicknesses of flexible inclusion, solid line for $h/h_0 = 0.0005$, dashed line for $h/h_0 = 0.5$ and dotted line for $h/h_0 = 0.75$ ($L/a=2.1$)

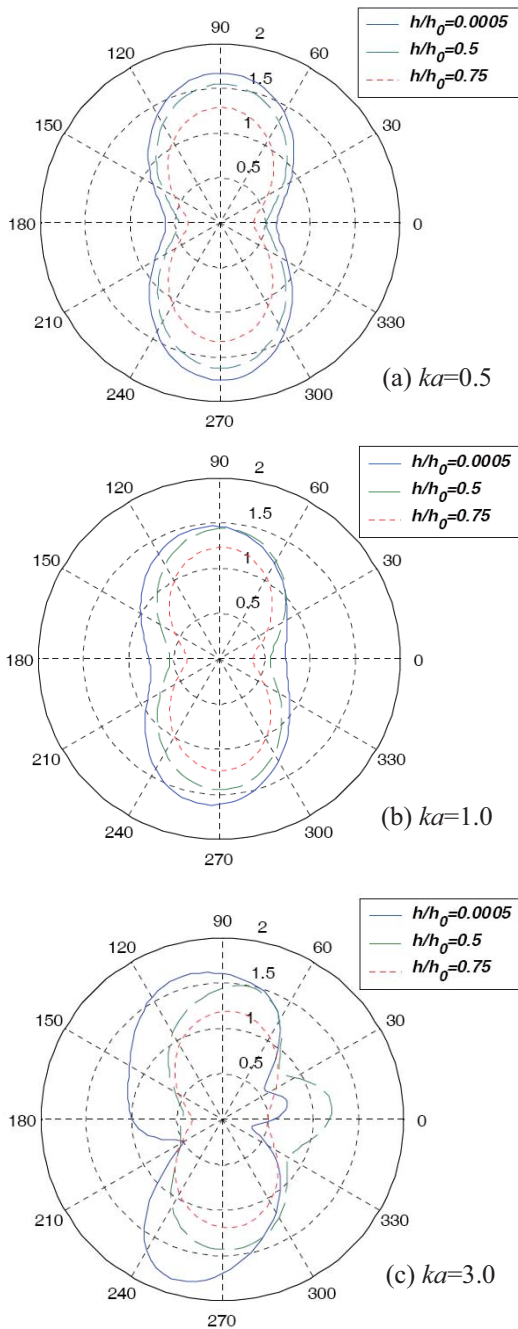


Figure 8 Distribution of DMCF on the first circular boundary B_1 at different thicknesses of flexible inclusion, solid line for $h/h_0 = 0.0005$, dashed line for $h/h_0 = 0.5$ and dotted line for $h/h_0 = 0.75$, and at different incident wave number (a) $ka=0.5$, (b) $ka=1.0$ and (c) $ka=3.0$ ($L/a=4.0$)

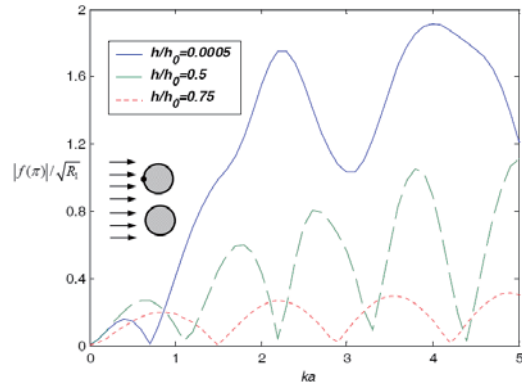


Figure 9 Far-field backscattering amplitude versus the dimensionless wave number at different thicknesses of flexible inclusion, solid line for $h/h_0 = 0.0005$, dashed line for $h/h_0 = 0.5$ and dotted line for $h/h_0 = 0.75$ ($L/a=4.0$)

多極 Trefftz 法求解含多圓形置入物薄板彎曲波散射

李為民¹, 陳正宗², 許宏和¹

¹ 中華科技大學機械工程系

² 國立臺灣海洋大學河海工程系

摘要

本文提出多極 Trefftz 法以求解含多圓形置入物之無限域薄板彎曲波散射問題。動應力集中係數 (Dynamic Moment Concentration Factor) 與遠場散射強度將利用解析推導並以數值計算求得。由於引入加法定理, 由多個座標系統所表示的解可轉換成由一個座標系統表示, 而該座標系統所在的圓邊界必須滿足連續條件。依此方式可求得一無限耦合線性代數系統作為含多圓形置入物之無限域薄板彎受入射彎曲波作用的解析模式。本文理論具有一般化特性可推廣至多圓形置入物問題。在捨去高次項的有限性代數系統中, 本文提出數個數值算例, 以探討入射波數、置入物厚度與置入物間距等因素對動應力集中係數與遠場散射強度的影響。數值結果顯示, 當置入物彼此相當接近時, 雙置入物的應力集中係數大於單置入物, 置入物間距對近場動應力集中係數與遠場散射強度有不同的影響。

關鍵詞: 散射, 薄板, 置入物, 彎曲波, 動應力集中係數, 遠場散射強度